SI APPENDIX

SUPPLEMENTARY FIGURES

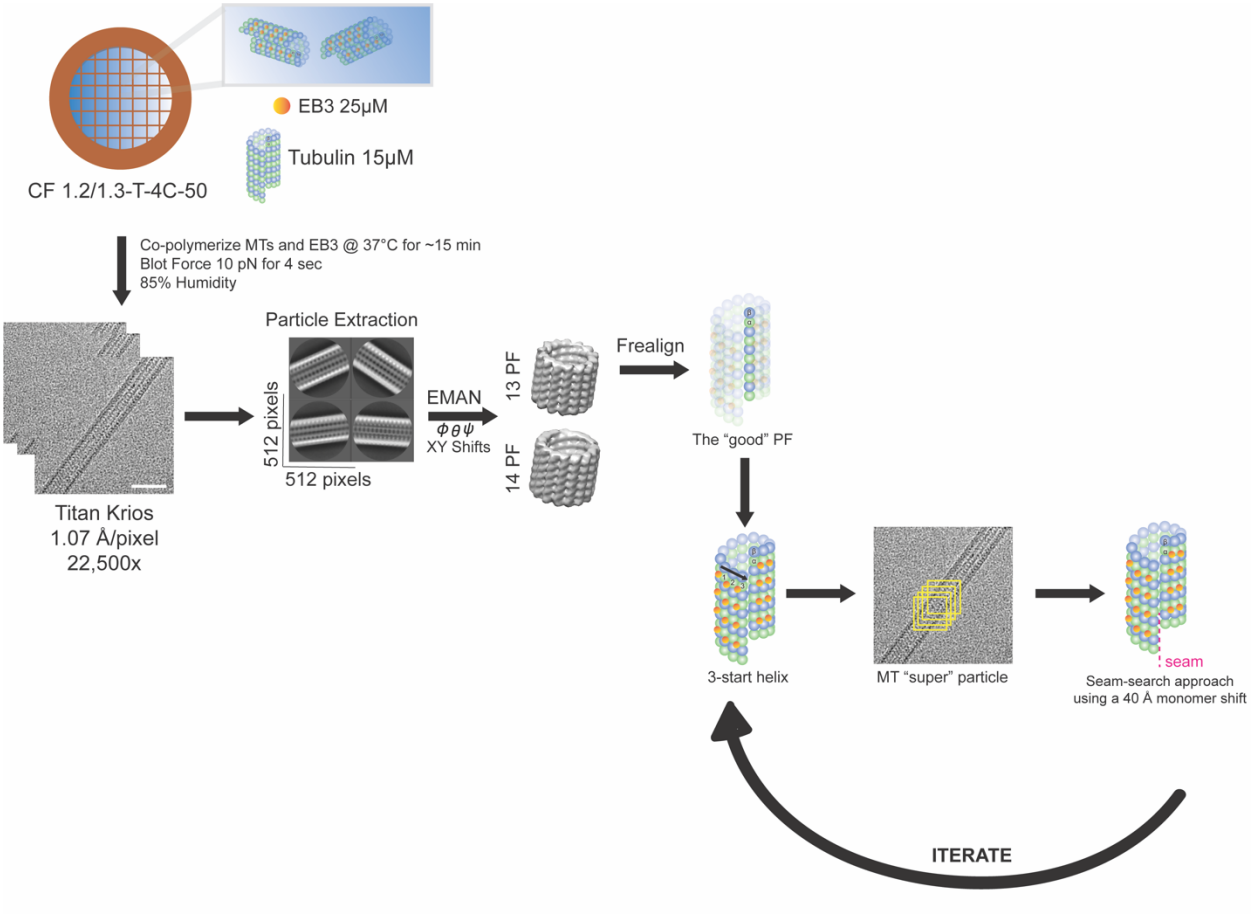

Supplemental Figure 1. Schematic of the experimental workflow for sample preparation and pseudo-helical image processing. EB3 decorated MTs were added to glow-discharged C-flat holey carbon grids (CF-1.2/1.3-4C, 400 mesh, Copper; Protochips, Morrisville, NC) inside a Vitrobot (FEI, Hillsboro, OR) set at 37°C and 85% humidity before plunge-freezing in ethane slush and liquid nitrogen. Images were collected with the Titan Krios electron microscope (Thermo Fisher Scientific, Inc., Waltham, MA) operated at 300kV and equipped with a K2 direct detector (Gatan, Pleasanton, CA). The micrographs were collected at a nominal magnification of

x22,500. Stacks of dose-fractionated image frames were aligned using the UCSF MotionCor2 software and CTF-corrected with CTFFIND4. MT segments were manually selected and converted to 90% overlapping boxes (512 × 512 pixels) for particle extraction. The remaining non-overlapping region is set to 80 Å and corresponds to the tubulin dimer repeat (asymmetric unit). These raw particles were compared to 2D projections of low-passed filtered MT models (~20 Å, 4° coarse angular step size) with 13 and 14 PFs using the multi-reference alignment (MRA) feature of EMAN1. Next, 13-PF MT particles were refined in FREALIGN v. 9.11 using pseudo-helical symmetry to account for the presence of the seam. To verify the location of the seam, MTs were categorized based on their azimuthal angle and refined again.

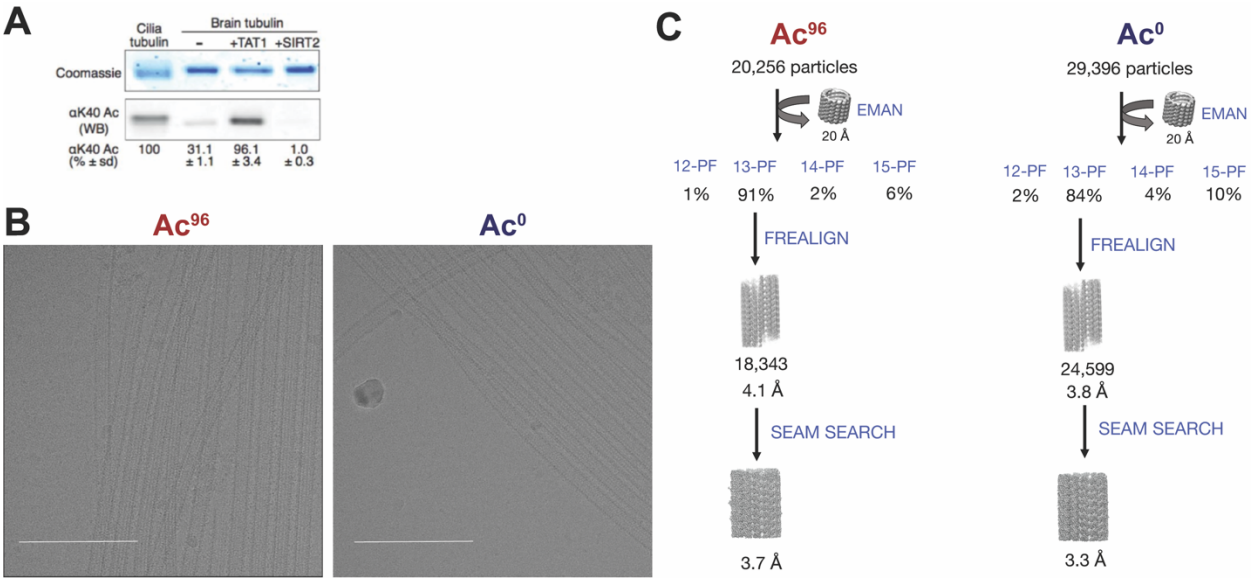

Supplemental Figure 2. Sample preparation, data collection and image processing of acetylated and deacetylated MT samples. (a) Ac^{96} and Ac^{0} tubulin preparations were produced by treating purified mammalian brain tubulin (Ac^{30}) with acetyltransferase αTAT1 and deacetylatase SIRT2. Samples were resolved on SDS-page and Coomassie-stained (top panel) or immunoblotted for αK40 acetylation (bottom panel). Axomenal preparations from Tetrahymena cilia provide a 100% acetylation calibrator. Adapted from Portran[1]. **(b)** Representative cryo-EM images of acetylated, in the left panel, and deacetylated MTs, in the right panel. Scale bar = 200 nm. Images were collected with the Titan Krios electron microscope (FEI, Hillsboro, OR) operated at 300kV and equipped with a K2 direct detector (Gatan, Pleasanton, CA). The micrographs were collected at a nominal magnification of 22,500x, resulting in a final pixel size of 1.07 Å per pixel and dose rate of 8 e-/pixel/s. **(c)** Schematic of data collection. Using EB3, we generated >80% homogeneous samples to push the resolution to ~3.5 Å.

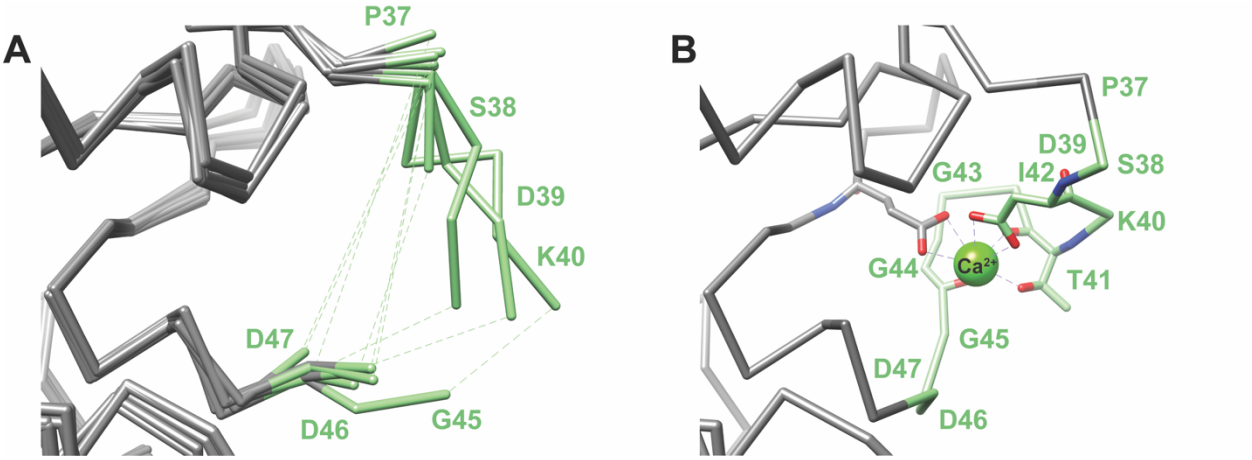

Supplemental Figure 3. Previous proposed αK40 loop models. (a) Published PDBs with incomplete models of the loop: 5NQU (Chain A), 5EYP (Chain A), 3RYC (Chain A), 3RYC (Chain C), 5NQT (Chain A), 3RYI (Chain A), 3RYI (Chain A), 3RYF (Chain A), 3RYF (Chain C). **(b)** Example of the a published PDB with the complete loop stabilized by calcium: 5YL4 (Chain C).

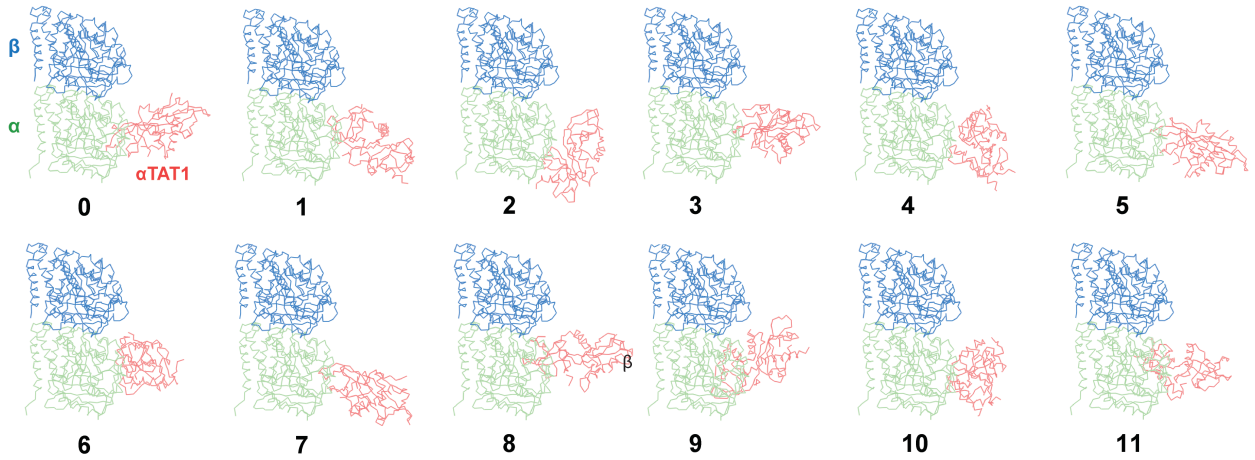

Supplemental Figure 4. **Proposed mechanism for αTAT1 intraluminal binding.** The α-carbon backbone of a bisubstrate analog containing α-tubulin residues 38-41 in complex with αTAT1 (PDB ID: 4PK3) is shown superimposed to representative αK40 loops of 12 clusters (0-11) from the metainference ensemble (β, sky blue; α, light green, αTAT1, deep salmon). All arrangements exhibit severe clashes between αTAT1 and the globular domain of α-tubulin, except cluster #2, which is highly enriched in Ac^0 samples and only has a single clash between αTAT1:R74 and α-tubulin G57.

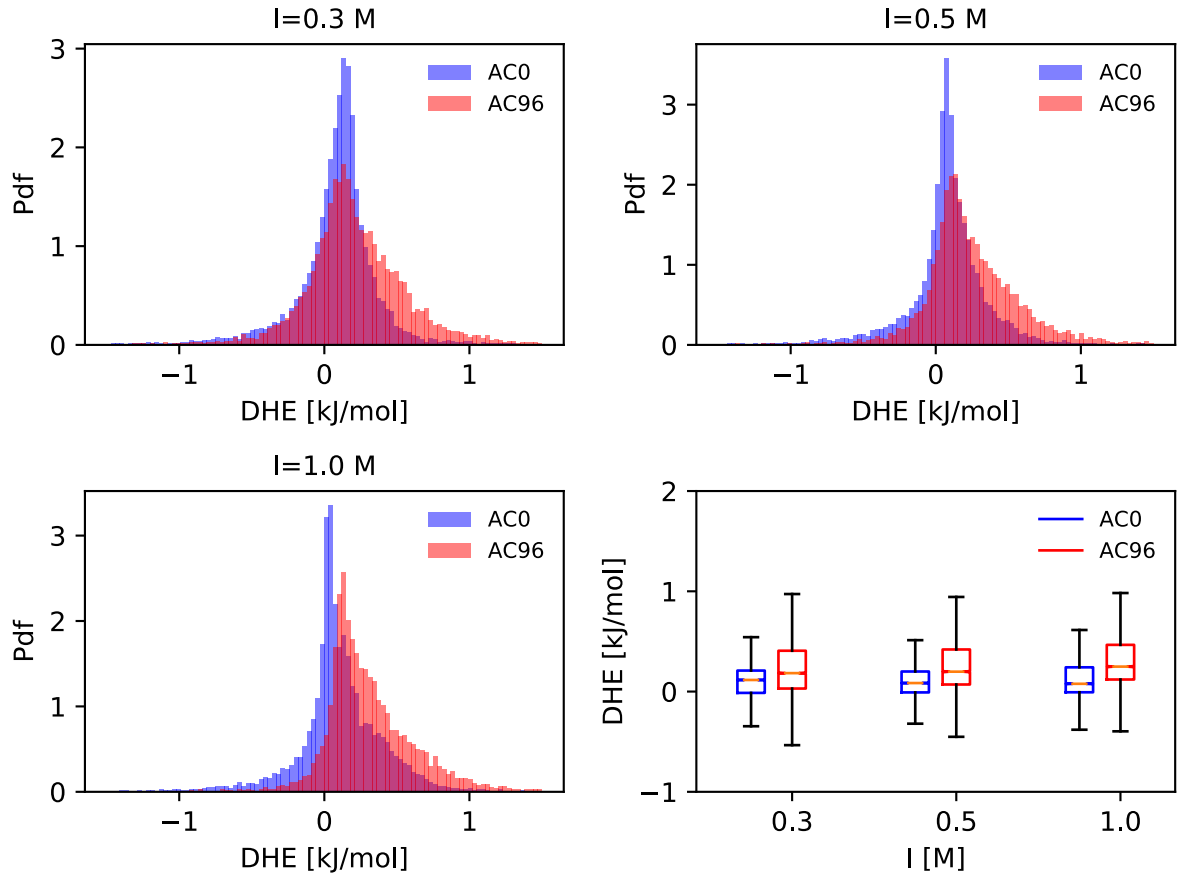

Supplemental Figure 5. Acetylation weakens lateral interactions. By analyzing the distribution of Debye-Hückel (DH) electrostatic energy between adjacent α-subunits across the Ac^0 (blue) and Ac^{96} ensembles (red), we find that acetylation weakens lateral interactions at multiple ionic strengths (0.3-1.0M). The DH energy is calculated between the following two groups of atoms: (i) all atoms in residue range 30-60 of chain A (α1 subunit) and (ii) all atoms in residue range 200-380 of chain E (α2 subunit) in PDBs 602S and 602T. The histograms show the probability density function as a function of the DH interaction energy and the whisker plots show the shifts in the means with quartile confidence intervals.

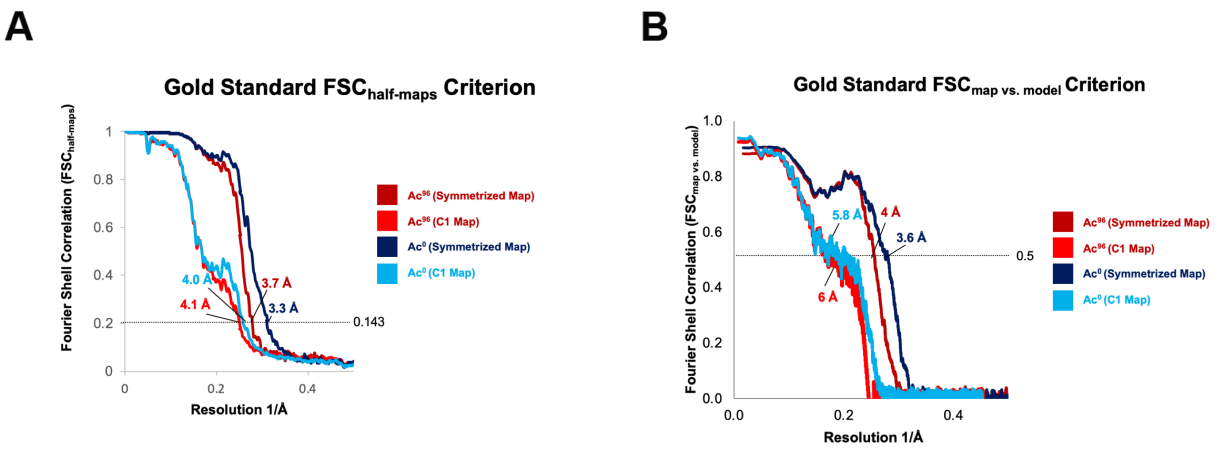

Supplemental Figure 6. Fourier Shell Correlation Plots.

The $FSC_{half\text{-}map}$ resolution, using **0.143** as the gold standard criterion, represents how well the two half-maps from each dataset correlate as a function of spatial frequency. The two half-maps were generated by dividing the final dataset into two independent 3D-reconstructions. The $FSC_{map\ vs.\ model}$ resolution, using **0.5** as the gold standard criterion, represents how well the final map correlated with the refined atomic model. All plots were generated in PHENIX.

SUPPLEMENTAL TABLE 1. CryoEM data collection, refinement parameters, and validation statistics.

Parameters	**Ac^{96} Symmetrized (EMDB-0612, PDB-602Q)**	**Ac^{0} Symmetrized (EMDB-0613, PDB-602R)**	**Ac^{96} C1 (EMDB-0615, PDB-602T)**	**Ac^{0} C1 (EMDB-0614, PDB-602S)**
Magnification	22500x	22500x	22500x	22500x
Voltage	300	300	300	300
Electron exposure (e-/A^2)	25	25	25	25
Defocus range (μm)	-1.5 to -2.5	-1.5 to -2.5	-1.5 to -2.5	-1.5 to -2.5
Pixel size (Å)	1.07 Å	1.07 Å	1.07 Å	1.07 Å
Symmetry imposed	HP	HP	C1	C1
Initial no. of images	287	871	287	871
Final no. of images	278	476	278	476
Initial no. of particles	20256	29396	20256	29396
Final no. of particles	18432	24692	18432	24692
Helical Rise			9.3	9.3
Helical Twist			27.7	27.7
Dimer Rise (Å)			80.5	81
Dimer Twist			-0.12º	-0.12º
Map resolution (Å)	**3.7**	**3.3**	**4.1**	**4.0**
FSC threshold	0.143	0.143	0.143	0.143
Map resolution range (Å)	3.5-4.1 Å	3.0-3.6 Å	3.8-5.4 Å	3.5-4.5 Å
Refinement				

Initial model used (PDB ID)	3JAR	3JAR	3JAR	3JAR
Model resolution (Å)	4 Å	3.6 Å	6 Å	5.8 Å
FSC threshold	0.5	0.5	0.5	0.5
Map sharpening method	*Phenix_auto_sharpen*	*Phenix_auto_sharpen*	*Phenix_auto_sharpen*	*Phenix_auto_sharpen*
Model composition				
Nonhydrogen atoms	40866	40866	320775	320775
Protein residues	5184	5184	40702	40702
Ligands (GTP, GDP)	12	12	94	94
B factors (Å^2)				
Protein	126.11	96.80	193.47	161.40
Ligand	122.25	89.44	192.42	156.32
Bond lengths: RMS (deviation)	0.007	0.007	0.007	0.006
Bond angles: RMS (deviation)	1.110	1.107	1.110	1.112
Validation				
MolProbity score	1.57	1.63	1.80	1.78
Clashscore	6.64	6.64	9.15	8.92
Rotamer outliers (%)	0.14	0.41	0.14	0.14
Ramachandran plot				
Favored (%)	96.74	96.18	95.48	95.6
Outliers (%)	0	0	0	0

87

88

Independent References Section

1. Portran, D., Schaedel, L., Xu, Z., Théry, M. & Nachury, M. V. Tubulin acetylation protects long-lived microtubules against mechanical ageing. *Nat. Cell Biol.* (2017). doi:10.1038/ncb3481